

Article

# Enhanced CO<sub>2</sub> Adsorption on Nitrogen-Doped Carbon Materials by Salt and Base Co-Activation Method

Ruiping Wei <sup>1,2</sup>, Xingchao Dai <sup>1,2</sup> and Feng Shi <sup>1,\*</sup>

<sup>1</sup> State Key Laboratory for Oxo Synthesis and Selective Oxidation, Lanzhou Institute of Chemical Physics, Chinese Academy of Sciences, No.18, Tianshui Middle Road, Lanzhou 730000, China; wei828111@163.com (R.W.); daixingchao@licp.cas.cn (X.D.)

<sup>2</sup> University of Chinese Academy of Sciences, No. 19A, Yuquan Road, Beijing 100049, China

\* Correspondence: fshi@licp.cas.cn; Tel.: +86-0931-4968142

Received: 20 February 2019; Accepted: 9 April 2019; Published: 12 April 2019



**Abstract:** Nitrogen-doped carbon materials with enhanced CO<sub>2</sub> adsorption were prepared by the salt and base co-activation method. First, resorcinol-formaldehyde resin was synthesized with a certain salt as an additive and used as a precursor. Next, the resulting precursor was mixed with KOH and subsequently carbonized under ammonia flow to finally obtain the nitrogen-doped carbon materials. A series of samples, with and without the addition of different salts, were prepared, characterized by XRD (X-ray powder diffraction), elemental analysis, BET (N<sub>2</sub>-adsorption-desorption analysis), XPS (X-ray photoelectron spectroscopy) and SEM (Scanning electron microscopy) and tested for CO<sub>2</sub> adsorption. The results showed that the salt and base co-activation method has a remarkable enhancing effect on the CO<sub>2</sub> capture capacity. The combination of KCl and KOH was proved to be the best combination, and 167.15 mg CO<sub>2</sub> could be adsorbed with 1 g nitrogen-doped carbon at 30 °C under 1 atm pressure. The materials characterizations revealed that the introduction of the base and salt could greatly increase the content of doped nitrogen, the surface area and the amount of formed micropore, which led to enhanced CO<sub>2</sub> absorption of the carbon materials.

**Keywords:** nitrogen-doped carbon materials; carbon dioxide adsorption; salt and base; co-activation method

## 1. Introduction

Terrible scenarios of global warming are attributed to the emission of built-up greenhouse gases. Among these greenhouse gases, carbon dioxide (CO<sub>2</sub>), released by the combustion of fuels and from certain industrial and resource extraction processes, is one of the main components. Thus, there are many concerns about reducing carbon dioxide in greenhouse gases. As a result, extensive research efforts have been undertaken to develop feasible materials for CO<sub>2</sub> capture [1]. Carbon dioxide adsorption especially by porous materials has become a hot research topic because these materials possess many advantages such as low energy requirements, quick and convenient processes of adsorption and desorption compared with chemical absorption [2]. In this context, many porous materials including zeolites [3–5], other inorganic molecular sieves [6–13], metal-organic frameworks [14–19] and carbon-based materials [20–24] have been investigated.

Among them, carbon-based materials are widely accepted as a promising candidate for CO<sub>2</sub> adsorption due to their chemical inertness, low cost, high surface area and tunable pore structures. The porous structure and high surface area of carbon materials allow the introduction of several functional groups on the surface to increase the capacity of CO<sub>2</sub> adsorption. Various carbon-based materials including metal-carbon composites [25], biowaste derived carbons [26–29] and nitrogen-doped carbons

(NC) [30–41] have been applied in CO<sub>2</sub> capture. Among them, nitrogen doped carbon materials have been reported to exhibit an excellent CO<sub>2</sub> capture capacity and high adsorption selectivity. The incorporation of nitrogen in carbon materials can greatly improve their CO<sub>2</sub> capture capacity by providing basic adsorption sites. In fact, besides nitrogen-doping, the CO<sub>2</sub> adsorption of carbon material could also be remarkably enhanced by base activation [42,43]. For example, nitrogen-free microporous materials [44–47] prepared by alkali etching have been demonstrated to be highly efficient in CO<sub>2</sub> adsorption. It is noteworthy that alkali etching usually led to the formation of a small amount of micropores and, in other words, the pore structure was changed. Thus, it brings a debate on the exact role of doped nitrogen and pore properties for CO<sub>2</sub> adsorption. Recently, it has been reported that the pore structure has a determining effect on CO<sub>2</sub> adsorption at lower temperature and lower pressure, while doped nitrogen plays an important role at higher temperature and higher pressure [48–50]. Therefore, it will be highly desirable to develop a porous carbon material enriched in nitrogen and dominated by micropores.

Based on the above discussions, here, we presented nitrogen-doped carbon materials with high CO<sub>2</sub> capture capacity, which were prepared by the salt and base co-activation method with resorcinol-formaldehyde resin as a precursor. The experimental results showed that the salt and base co-activation method could greatly improve the CO<sub>2</sub> capture capacity of nitrogen-doped carbon material. The characterization analysis revealed an obvious increase of the doped nitrogen content and the amount of the micropores formed in the carbon material prepared by the salt and base co-activation method, which might be the reason for the enhancement of CO<sub>2</sub> adsorption. Therefore, a conclusion could be drawn that CO<sub>2</sub> adsorption was determined by both micropores and the doped nitrogen.

## 2. Materials and Methods

### 2.1. Materials Preparation

Precursors of carbon materials were synthesized by a low temperature hydro-thermal method according to the reported references [51–53]. The precursor applied was synthesized as following: Typically, resorcinol (R, 2.20 g, 20 mmol), formaldehyde (F, 3.25 g, 40 mmol, 37 wt % aqueous solution) and 9 mL deionized water were added into a 100 mL Teflon® autoclave. Subsequently, 21.2 mg Na<sub>2</sub>CO<sub>3</sub> (1 mol % relative to resorcinol) and 0.25–1.25 g salts (KCl, KNO<sub>3</sub>, NaCl, NaNO<sub>3</sub>, Na<sub>2</sub>SO<sub>4</sub>) were added into the autoclave. The mixture was stirred for 1 h at room temperature, and then the autoclave was sealed and kept at 80 °C for 24 h and cooled it down to room temperature to provide an R-F resin (R: resorcinol and F: formaldehyde). The wet resin was put into a round-bottom flask and dried at 130 °C in vacuum condition for 3 h and used as the carbon precursor. Precursor without salt additive was prepared through the same process. Next, the synthesized precursors were mixed mechanically with KOH (0.4–2.0 g) and then carbonized at 400–700 °C (a heating rate of 10 °C min<sup>-1</sup>) for 3 h under ammonia flow (20 mL min<sup>-1</sup>). The resulting carbon materials were ultrasonically washed with deionized water (about 300 mL) until pH ≈ 7.0 and then dried at 80 °C for 6 h to provide the final sample.

### 2.2. CO<sub>2</sub> Adsorption Measurements

CO<sub>2</sub> adsorption of the carbon materials was measured using a Mettler-Toledo SDTA851 thermogravimetric analyzer according to the reported references [54–56]. In detail, firstly, 10 mg of sample was placed in a porcelain crucible with the volume of 0.1 mL. When the temperature reached 30 °C, the program was started with carbon dioxide (99.9%) as the reaction gas at a flow of 60 mL min<sup>-1</sup> under 1 atm pressure, and held at that temperature for 50 min. After the completion of the adsorption, the mass of samples after CO<sub>2</sub> adsorption was recorded as  $m_1$ . Subsequently, the reaction gas was switched to nitrogen (99.9%) with the same flow rate, and at the same time the temperature was increased to 200 °C at a rate of 10 °C min<sup>-1</sup> and held for 30 min to ensure the complete removal of

CO<sub>2</sub> that samples' adsorbed. After that, the mass of samples was recorded as  $m_0$ , which is used as the true mass of the sample. CO<sub>2</sub> adsorption capacity could be calculated by  $m_1$  and  $m_0$ .

### 2.3. Characterization Techniques

X-ray powder diffraction (XRD) was performed on a Rigaku D/max-2400 X-ray diffractometer (Rigaku, Tokyo, Japan) with Ni-filtered Cu K $\alpha$  radiation at 40 kV and 100 mA. The XRD patterns were scanned in the  $2\theta$  range of 10–80°.

Elemental analysis (C, N, H and O) of the samples was carried out on a Vario EL microanalyzer (Elementar, Hanau, Germany).

X-ray photoelectron spectroscopy (XPS) was performed by using a Thermo Scientific ESCALAB 250 instrument (Thermo Fisher Scientific, Waltham, MA, USA) with a dual Mg/Al anode X-ray source, a hemispherical capacitor analyser and a 5 keV Ar<sup>+</sup> ion-gun. All of the spectra were recorded using non-monochromatic Mg K $\alpha$  ( $h\nu = 1253.6$  eV) radiation.

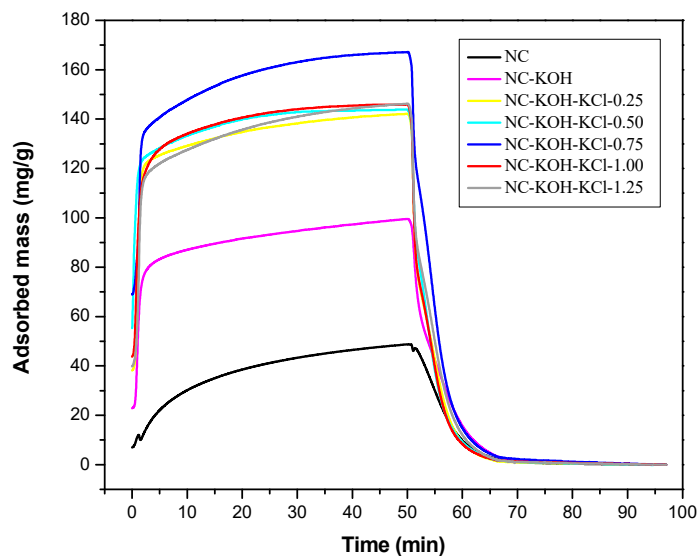
The specific surface area ( $S_{BET}$ ) was calculated using the Brunauer–Emmett–Teller (BET) equation with a relative pressure of 0.05–0.30. The total pore volume ( $V_{Total}$ ) was obtained at the maximum incremental volume point. Micropore volume was determined from the Dubinin–Radushkevich equation. Mesoporous volume was determined by the subtraction of micropore volume from the total pore volume. Fraction of micropore volume = (micropore volume/total pore volume) \* 100. The micropore size distribution was calculated by the Harvath–Kawazoe (H–K) equation based on the N<sub>2</sub>/77 K adsorption data.

SEM was performed with a JEOL JSM-6701F (JEOL, Tokyo, Japan) equipped with a cold FEG (Field Emission Gun).

## 3. Results and Discussion

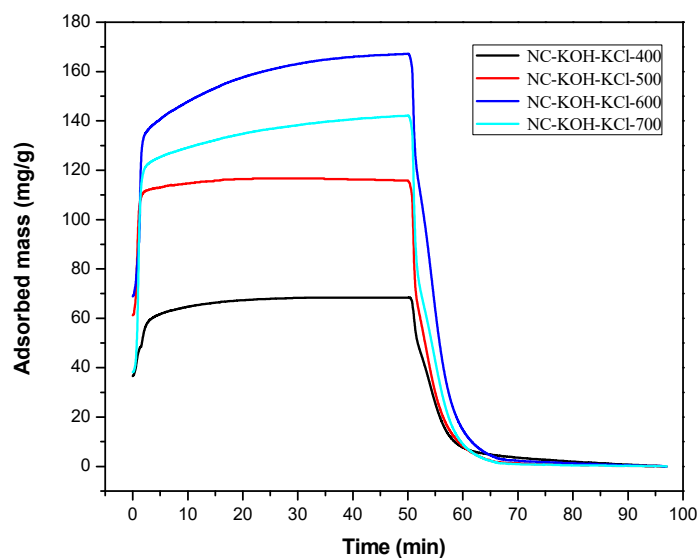
### 3.1. CO<sub>2</sub> Adsorption Performance Test

Figure 1 showed the TG curves of CO<sub>2</sub> adsorption and desorption of these samples activated with 1.2 g KOH and different amount of KCl from 0 to 1.25 g with an interval of 0.25g per 2.20 g resorcinol. The CO<sub>2</sub> adsorption-desorption behavior was measured at 30 °C under 1 atm. On the basis of the amount of KCl added, these samples were denoted as NC-KOH, NC-KOH-KCl-0.25, NC-KOH-KCl-0.50, NC-KOH-KCl-0.75, NC-KOH-KCl-1.00 and NC-KOH-KCl-1.25. The unactivated sample was denoted as NC. All these samples were carbonized at 600 °C for 3 h under ammonia flow (20 mL min<sup>-1</sup>). It can be seen from the Figure 1, all the samples adsorbed CO<sub>2</sub> rapidly at the beginning, then continued with a slower rate and reached an equilibrium in 50 min. During the desorption process, the adsorbed CO<sub>2</sub> is removed rapidly and the mass of samples gradually decreased until a constant value was reached at 200 °C. Figure 1 showed that NC sample had the lowest CO<sub>2</sub> adsorption capacity and a higher CO<sub>2</sub> adsorption capacity was observed in the case of NC-KOH sample, which suggested that the introduction of the base in the carbonization process has a positive effect on the increase of CO<sub>2</sub> adsorption capacity. Similar effect could be also observed by adding the salt in the R-F resin synthesis. Among the tested samples, the samples activated by base and salt exhibited best ability in the CO<sub>2</sub> adsorption, which could be attributed to the synergistic effect of base and salt pretreatment. However, there is no a linear correlation between the CO<sub>2</sub> adsorption capacity of the sample and the amount of the salt added. The CO<sub>2</sub> adsorption capacity of the sample firstly increased then declined, and the maximum (167.15 mg/g) was observed when the sample was activated with 0.75 g KCl and 1.2 g KOH.



**Figure 1.** TG curves measured CO<sub>2</sub> adsorption and desorption of samples activated by different amount of KCl and 1.2 g KOH per 2.20 g resorcinol.

After optimizing the amount of KCl, the carbonization temperature of the NC-KOH-KCl-0.75 sample was further optimized in the range of 400–700 °C and the results were shown in the Figure 2. With the increase of the carbonization temperature from 400–600 °C, the CO<sub>2</sub> adsorption capacity of the sample was gradually enhanced, but a drop was observed when the temperature reached at 700 °C. The best CO<sub>2</sub> adsorption performance was obtained when the NC-KOH-KCl-0.75 sample was carbonized at 600 °C.



**Figure 2.** TG curves measured CO<sub>2</sub> adsorption and desorption of samples carbonized at different temperatures.

Following the above results, the effect of the salt kind was investigated (Figure 3). A series of different salts such as KNO<sub>3</sub>, NaNO<sub>3</sub>, KCl, NaCl and Na<sub>2</sub>SO<sub>4</sub> were added in the R-F resin synthesis process with the optimized amount of 0.75 g and all the samples were carbonized at 600 °C. The results showed that the kind of the salt added has a great effect on the CO<sub>2</sub> adsorption capacity of the sample. The highest CO<sub>2</sub> adsorption capacity was obtained when the NC-KOH-KCl sample was used, and 167.15 mg CO<sub>2</sub> could be adsorbed with 1 g NC-KOH-KCl sample. Slight or much lower values were

observed when the other salts such as  $\text{KNO}_3$ ,  $\text{NaNO}_3$ ,  $\text{NaCl}$  and  $\text{Na}_2\text{SO}_4$  were used. Among all the samples tested, the  $\text{CO}_2$  adsorption capacity of the sample activated by  $\text{Na}_2\text{SO}_4$  was the lowest.

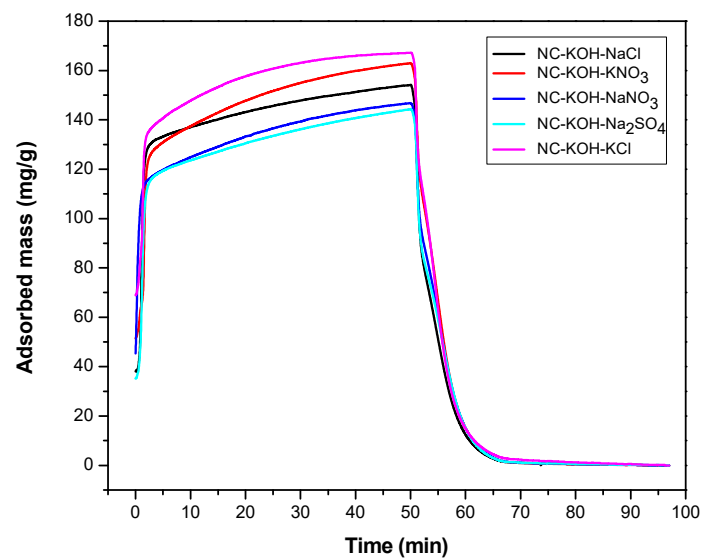


**Figure 3.** TG curves measured  $\text{CO}_2$  adsorption and desorption of samples activated by different salts.

Finally, the amount of KOH added in the carbonization process was optimized in the range of 0–2.0 g and a series of samples activated with 0.75 g KCl and different amounts of KOH were prepared. The results in the Figure 4 showed that the  $\text{CO}_2$  adsorption capacity of the NC-KCl-KOH-0.4 sample was much higher than that of the sample activated only with KCl, which indicated that the introduction of KOH could greatly increase the  $\text{CO}_2$  adsorption capacity of the sample. Further increasing the amount of KOH led to higher  $\text{CO}_2$  adsorption capacity, but a sudden drop was observed when 1.6 g KOH was added. The decreased tendency could also be observed when further increasing the amount of KOH to 2.0 g.

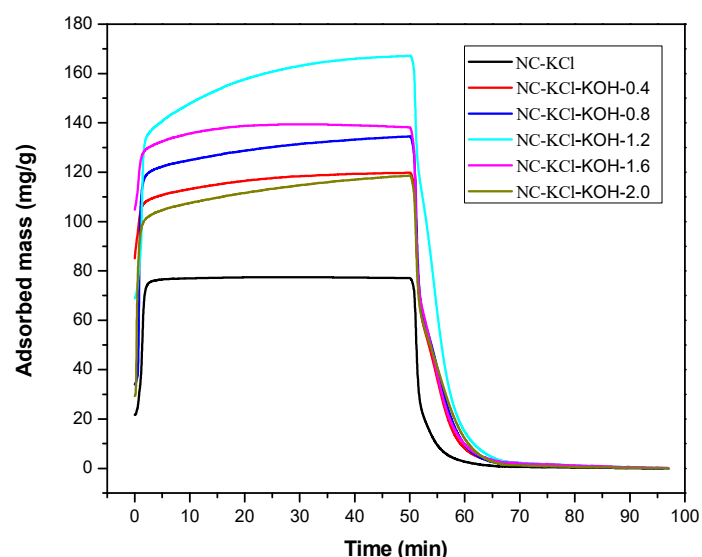


**Figure 4.** TG curves measured  $\text{CO}_2$  adsorption and desorption of samples activated by different amount of KOH and 0.75 g KCl per 2.20 g resorcinol.

In order to better illuminate the effect of salt and base activation on the  $\text{CO}_2$  adsorption capacity of nitrogen-doped carbon materials, four typical samples, e.g., NC, NC-KCl, NC-KOH and NC-KCl-KOH were chosen and further compared (Figure 5). In comparison with NC, NC-KCl and NC-KOH both

exhibited better CO<sub>2</sub> adsorption capacity, which indicated that the base and salt pretreatment both had a promoted effect on the CO<sub>2</sub> adsorption capacity of the carbon materials, but base is superior to salt by contrast. The highest CO<sub>2</sub> adsorption capacity was obtained when the NC sample was activated by the combination of base and salt, which could be attributed the synergistic effect of base and salt added in the different steps.

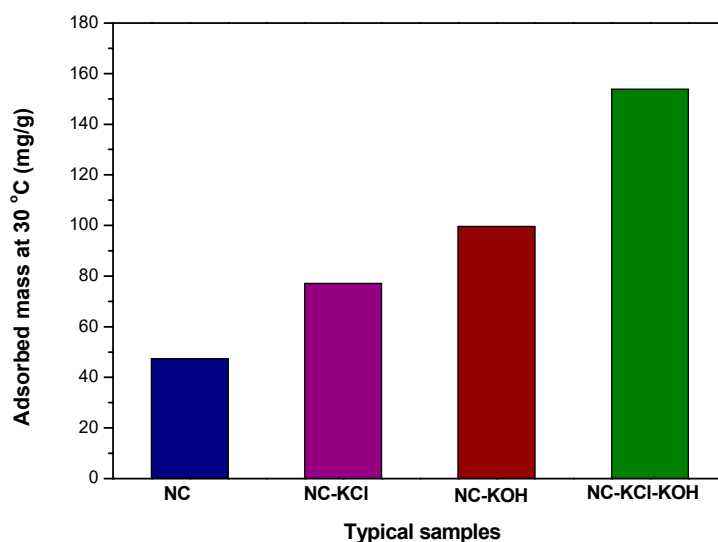


**Figure 5.** Values of typical samples'CO<sub>2</sub> adsorption measured by TGA at 30 °C under 1 atm pressure.

### 3.2. Characterization Results and Discussion

In order to explore the relationship of structure and performance, the prepared samples were characterized by elemental analysis and N<sub>2</sub>-adsorption-desorption analysis, and the results are shown in Tables 1 and 2, and Figure 6. Obviously, the NC-KOH-KCl-0.75 sample has the highest nitrogen content (12.59 wt %), which implied that the doped nitrogen could promote the CO<sub>2</sub> adsorption (Table 1). The N<sub>2</sub>-adsorption-desorption analysis revealed that the NC-KOH-KCl-0.75 sample has the largest specific surface areas and highest fraction of micropore volume to total pore volume, which means that the large specific area and more micropores formation might favors the CO<sub>2</sub> adsorption (Table 2). Thus, the CO<sub>2</sub> adsorption performance of the carbon material could be affected by the content of the doped nitrogen, the specific area and the amount of micropores.

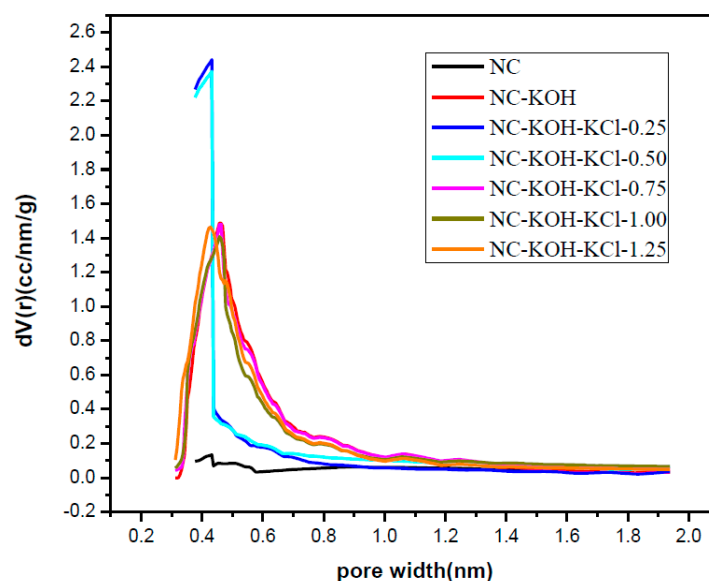
**Table 1.** The content of N, C, H and O in samples activated by different amount of KCl and 1.2 g KOH per 2.20 g resorcinol.

Samples	N (wt %)	C (wt %)	H (wt %)	O (wt %)
NC	7.78	76.12	1.91	14.19
NC-KOH	11.99	58.22	2.67	27.12
NC-KOH-KCl-0.25	7.05	69.19	1.76	22.00
NC-KOH-KCl-0.50	8.40	70.09	1.88	19.63
NC-KOH-KCl-0.75	12.59	56.23	2.58	28.60
NC-KOH-KCl-1.00	9.43	68.05	1.88	20.64
NC-KOH-KCl-1.25	8.70	66.12	1.74	23.44

**Table 2.** BET surface area and porosity of samples activated by different amount of KCl and 1.2 g KOH per 2.20 g resorcinol.

Samples	$S_{BET}$ ( $m^2 g^{-1}$ ) <sup>1</sup>	$V_{total}$ ( $cm^3 g^{-1}$ ) <sup>2</sup>	$V_{Micro}$ ( $cm^3 g^{-1}$ ) <sup>3</sup>	$V_{Meso}$ ( $cm^3 g^{-1}$ ) <sup>4</sup>	$F_{Micro}$ (%) <sup>5</sup>
NC	158	0.190	0.055	0.135	29
NC-KOH	1030	0.659	0.401	0.258	61
NC-KOH-KCl-0.25	911	1.013	0.354	0.659	35
NC-KOH-KCl-0.50	900	0.573	0.349	0.224	61
NC-KOH-KCl-0.75	1034	0.634	0.398	0.236	63
NC-KOH-KCl-1.00	858	0.740	0.361	0.379	49
NC-KOH-KCl-1.25	1006	0.615	0.389	0.226	63

<sup>1</sup>  $S_{BET}$  is the specific surface areas determined by the BET method. <sup>2</sup>  $V_{Total}$  is the total pore volume. <sup>3</sup>  $V_{Micro}$  is the micropore volume. <sup>4</sup>  $V_{Meso}$  is the mesoporous volume. <sup>5</sup>  $F_{Micro}$  is the fraction of micropore volume to total pore volume.

**Figure 6.** The micropore size distribution of samples activated by different amount of KCl and 1.2 g KOH per 2.20 g resorcinol.

Then, the effect of carbonized temperature on the structure was investigated by the elemental analysis and  $N_2$ -adsorption-desorption analysis. It can be seen from the elemental analysis results shown in Table 3 that higher carbonized temperature led to more doped nitrogen in the range of 400–700 °C and the content of doped nitrogen could be increased from 3.5 wt % to 13.08 wt % (Table 3). The NC-KOH-KCl-700 sample has the highest nitrogen content, but its  $CO_2$  adsorption capacity is not the highest, which means that the  $CO_2$  adsorption capacity of the carbon material was not determined by only the content of the doped nitrogen. Further,  $N_2$ -adsorption-desorption analysis revealed a good correlation between the micropore volume and the carbonized temperature. In addition, micropore volume enlarged with the increase of the carbonized temperature (Table 4 and Figure 7). The NC-KOH-KCl-600 sample with the best  $CO_2$  adsorption performance has the highest fraction of micropore volume to total pore volume, which is consistent with the above discussions.

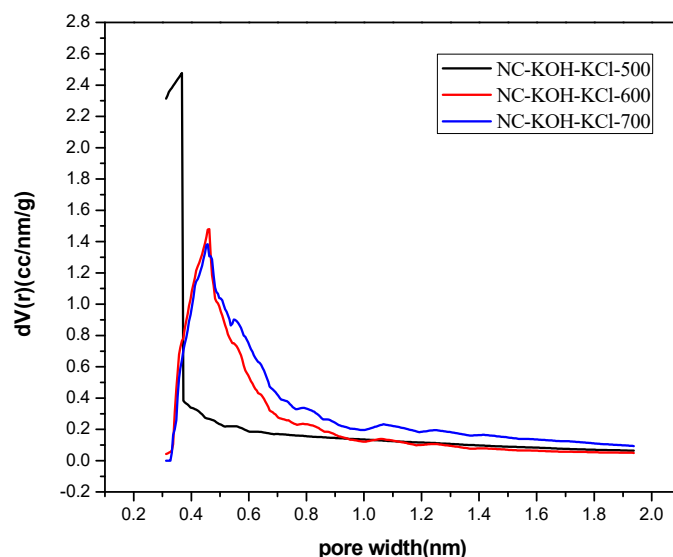
**Table 3.** The content of N, C, H and O in samples carbonized at different temperatures.

Samples	N (wt %)	C (wt %)	H (wt %)	O (wt %)
NC-KOH-KCl-400	3.5	66.00	2.13	28.37
NC-KOH-KCl-500	7.74	69.58	1.84	20.84
NC-KOH-KCl-600	12.59	56.23	2.58	28.60
NC-KOH-KCl-700	13.08	63.95	1.30	21.67

**Table 4.** BET surface area and porosity of samples carbonized at different temperatures.

Samples	$S_{\text{BET}}$ ( $\text{m}^2 \text{g}^{-1}$ ) <sup>1</sup>	$V_{\text{total}}$ ( $\text{cm}^3 \text{g}^{-1}$ ) <sup>2</sup>	$V_{\text{Micro}}$ ( $\text{cm}^3 \text{g}^{-1}$ ) <sup>3</sup>	$V_{\text{Meso}}$ ( $\text{cm}^3 \text{g}^{-1}$ ) <sup>4</sup>	$F_{\text{Micro}}$ (%) <sup>5</sup>
NC-KOH-KCl-400	167	0.210	0.009	0.201	4
NC-KOH-KCl-500	959	0.671	0.369	0.302	55
NC-KOH-KCl-600	1034	0.634	0.398	0.236	63
NC-KOH-KCl-700	1300	0.812	0.483	0.329	59

<sup>1</sup>  $S_{\text{BET}}$  is the specific surface areas determined by the BET method. <sup>2</sup>  $V_{\text{Total}}$  is the total pore volume. <sup>3</sup>  $V_{\text{Micro}}$  is the micropore volume. <sup>4</sup>  $V_{\text{Meso}}$  is the mesoporous volume. <sup>5</sup>  $F_{\text{Micro}}$  is the fraction of micropore volume to total pore volume.

**Figure 7.** The micropore size distribution of samples carbonized at different temperatures.

Next, the samples activated by KOH and different salts were characterized by elemental analysis and  $\text{N}_2$ -adsorption-desorption analysis and the results were shown in Tables 5 and 6 and Figure 8. Obviously, these samples co-activated by base and salt have high nitrogen content and all exceeded 12 wt % (Table 5). Especially, for the samples activated by  $\text{KNO}_3$ ,  $\text{NaNO}_3$  and  $\text{Na}_2\text{SO}_4$ , the nitrogen content above 15 wt % was observed. The  $\text{N}_2$ -adsorption-desorption analysis revealed that the kind of the activated salt has a great effect on the pore structure of the carbon material. The samples activated by KCl and NaCl exhibited a specific surface area above  $1000 \text{ m}^2 \text{g}^{-1}$  while the smaller specific surface area than  $1000 \text{ m}^2 \text{g}^{-1}$  were observed in the case of other salts (Table 6). Similar phenomena were also observed in the case of total pore volume and micropore volume. It is noteworthy that the NC-KOH-KCl sample exhibited the highest fraction of micropore volume to total pore volume although its micropore volume is not the largest, which suggested that a larger micropore volume did not mean higher  $\text{CO}_2$  adsorption capacity.

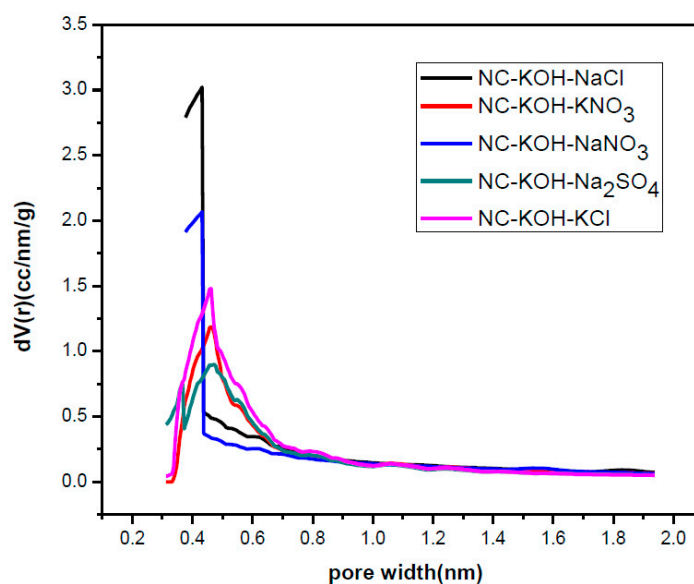
**Table 5.** The content of N, C, H and O in samples activated by different salts.

Samples	N (wt %)	C (wt %)	H (wt %)	O (wt %)
NC-KOH-NaCl	12.27	59.51	1.53	26.69
NC-KOH- $\text{KNO}_3$	15.45	56.01	1.51	27.03
NC-KOH- $\text{NaNO}_3$	15.37	67.18	1.57	15.88
NC-KOH- $\text{Na}_2\text{SO}_4$	15.22	58.14	1.71	24.93
NC-KOH-KCl	12.59	56.23	2.58	28.60

**Table 6.** BET surface area and porosity of samples activated by different salts.

Samples	$S_{\text{BET}}$ ( $\text{m}^2 \text{g}^{-1}$ ) <sup>1</sup>	$V_{\text{total}}$ ( $\text{cm}^3 \text{g}^{-1}$ ) <sup>2</sup>	$V_{\text{Micro}}$ ( $\text{cm}^3 \text{g}^{-1}$ ) <sup>3</sup>	$V_{\text{Meso}}$ ( $\text{cm}^3 \text{g}^{-1}$ ) <sup>4</sup>	$F_{\text{Micro}}$ (%) <sup>5</sup>
NC-KOH-NaCl	1217	0.775	0.466	0.309	60
NC-KOH-KNO <sub>3</sub>	874	0.629	0.327	0.302	52
NC-KOH-NaNO <sub>3</sub>	854	0.620	0.323	0.297	52
NC-KOH-Na <sub>2</sub> SO <sub>4</sub>	926	0.602	0.354	0.248	59
NC-KOH-KCl	1034	0.634	0.398	0.236	63

<sup>1</sup>  $S_{\text{BET}}$  is the specific surface areas determined by the BET method. <sup>2</sup>  $V_{\text{Total}}$  is the total pore volume. <sup>3</sup>  $V_{\text{Micro}}$  is the micropore volume. <sup>4</sup>  $V_{\text{Meso}}$  is the mesoporous volume. <sup>5</sup>  $F_{\text{Micro}}$  is the fraction of micropore volume to total pore volume.

**Figure 8.** The micropore size distribution of samples activated by different salts.

Furthermore, in order to explore the difference in the structure of the samples activated by different amount of KOH, these samples were characterized by elemental analysis and N<sub>2</sub>-adsorption-desorption analysis and the results were shown in Tables 7 and 8 and Figure 9. The elemental analysis showed that the nitrogen content in the NC-KCl sample was 5.28 wt % and the value could be increased to 11.2 wt % by adding 0.4 g KOH (Table 7), which implied that the introduction of KOH could greatly increase the nitrogen content. The addition of more KOH led to higher nitrogen content, but slight-promotion effect was observed if the amount of KOH exceeded 1.2 g. Besides, the promotion effect of KOH was also observed in the specific area. Apart from the NC-KCl-KOH-0.4 sample (Table 8), all the other samples activated by KOH exhibited a larger specific area than the NC-KCl sample, which suggested that the introduction of KOH could increase the specific area of the carbon material, but a certain amount of KOH was required.

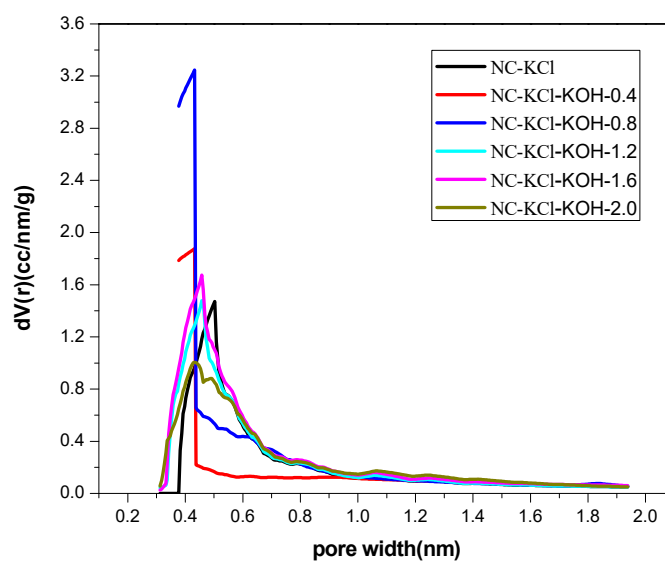
**Table 7.** The content of N, C, H and O in samples activated by different amount of KOH and 0.75g KCl per 2.20 g resorcinol.

Samples	N (wt %)	C (wt %)	H (wt %)	O (wt %)
NC-KCl	5.28	65.28	2.51	26.93
NC-KCl-KOH-0.4	11.2	73.27	1.4	14.13
NC-KCl-KOH-0.8	12.54	61.97	1.39	24.1
NC-KCl-KOH-1.2	12.59	56.23	2.58	28.60
NC-KCl-KOH-1.6	12.65	63.23	1.54	22.58
NC-KCl-KOH-2.0	12.96	58.89	1.4	26.75

**Table 8.** BET surface area and porosity of samples activated by different amount of KOH and 0.75g KCl per 2.20 g resorcinol.

Samples	$S_{BET}$ ( $m^2 g^{-1}$ ) <sup>1</sup>	$V_{total}$ ( $cm^3 g^{-1}$ ) <sup>2</sup>	$V_{Micro}$ ( $cm^3 g^{-1}$ ) <sup>3</sup>	$V_{Meso}$ ( $cm^3 g^{-1}$ ) <sup>4</sup>	$F_{Micro}$ (%) <sup>5</sup>
NC-KCl	903	0.686	0.348	0.338	51
NC-KCl-KOH-0.4	702	0.518	0.269	0.249	52
NC-KCl-KOH-0.8	1352	0.758	0.517	0.241	68
NC-KCl-KOH-1.2	1034	0.634	0.398	0.236	63
NC-KCl-KOH-1.6	1159	0.722	0.445	0.277	62
NC-KCl-KOH-2.0	999	0.575	0.377	0.198	66

<sup>1</sup>  $S_{BET}$  is the specific surface area determined by the BET method. <sup>2</sup>  $V_{Total}$  is the total pore volume. <sup>3</sup>  $V_{Micro}$  is the micropore volume. <sup>4</sup>  $V_{Meso}$  is the mesoporous volume. <sup>5</sup>  $F_{Micro}$  is the fraction of micropore volume to total pore volume.

**Figure 9.** The micropore size distribution of samples activated by different amount of KOH and 0.75 g KCl per 2.20 g resorcinol.

XRD patterns of the sample were shown in the Figure 10 and a typical reflection of amorphous carbon at about  $24^\circ$  was observed in all samples, which could be assigned to hexagonal graphite [47]. Besides, a weak peak appeared at approximately  $43^\circ$  in all the samples but NC-KCl-KOH sample, which could be assigned to rhombohedral graphite [47]. By correlating with the  $CO_2$  adsorption capacity, it's not difficult to make a speculation that the formation of rhombohedral graphite might produce adverse effect for the  $CO_2$  adsorption.

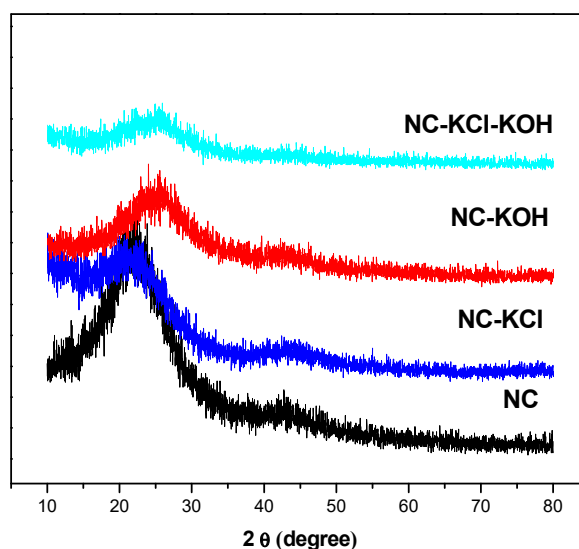


Figure 10. X-ray diffraction patterns of typical samples.

The contents of C, H and N in the sample were determined by elemental analysis, and the content of O was calculated by the subtracting from the content of C, H and N from the total content. The results in Table 9 showed that the activation of the sample by base and salt has a great effect on the content of N. The nitrogen content in the NC sample was 7.78 wt %, and the value could be increased to 11.99 wt % by the KOH activation, which suggested that the introduction of KOH might favors the formation of nitrogen-containing functional groups during ammoxidation process. As is well known, the existence of the doped nitrogen could provide the basic sites to adsorb CO<sub>2</sub> and higher nitrogen content means more CO<sub>2</sub> adsorption sites. Therefore, the higher CO<sub>2</sub> adsorption capacity of the NC-KOH exhibited could be well explained. A similar increase in the nitrogen was observed when the sample was activated by KOH and KCl, which further confirmed the effect of KOH. Considering the enhanced CO<sub>2</sub> adsorption capacity of NC-KOH and NC-KCl-KOH samples in comparison with NC, a speculation could be made that the high nitrogen content in the sample is good for the CO<sub>2</sub> adsorption by providing more basic sites. It is worth noting that the nitrogen content of the sample activated by KCl decreased, but its CO<sub>2</sub> adsorption capacity reversely increased, which implied that the introduction of KCl might increase the CO<sub>2</sub> adsorption capacity by changing the sample's pore structures not increasing the nitrogen content.

Table 9. The content of N, C, H and O in the typical samples determined by elemental analysis.

Samples	N (wt %)	C (wt %)	H (wt %)	O (wt %)
NC	7.78	76.12	1.91	14.19
NC-KCl	5.28	65.28	2.51	26.93
NC-KOH	11.99	58.22	2.67	27.12
NC-KCl-KOH	12.59	56.23	2.58	28.60

Then the porosity and BET specific surface area of typical samples were determined by N<sub>2</sub> adsorption and desorption and the results are shown in Table 10. Obviously, the samples activated by KOH and/or KCl had a larger surface area than the NC sample, and the NC-KCl-KOH sample with the highest CO<sub>2</sub> adsorption capacity exhibited the largest surface area, which suggested that the large surface area might be favorable the CO<sub>2</sub> adsorption. A similar phenomenon could also be observed in the pore volume of the sample and the pore volume of the sample could be increased from 0.19 cm<sup>3</sup> g<sup>-1</sup> to 0.634 cm<sup>3</sup> g<sup>-1</sup> by the co-activation of KOH and KCl. However, the NC-KCl sample showed the biggest pore volume although its CO<sub>2</sub> adsorption capacity was lower than that of the NC-KOH and NC-KCl-KOH samples. In order to gain more insights on the correlation of the pore volume

and the CO<sub>2</sub> adsorption capacity, the micropore and mesoporous volume as well as the fraction of micropore volume to total pore volume were calculated, respectively. A linear correlation between the CO<sub>2</sub> adsorption capacity and the fraction of micropore volume to total pore volume could be observed, which suggested that the formation of the micropore should be important for the CO<sub>2</sub> adsorption.

**Table 10.** BET surface area and porosity of typical samples.

Samples	$S_{\text{BET}}$ ( $\text{m}^2 \text{g}^{-1}$ ) <sup>1</sup>	$V_{\text{total}}$ ( $\text{cm}^3 \text{g}^{-1}$ ) <sup>2</sup>	$V_{\text{Micro}}$ ( $\text{cm}^3 \text{g}^{-1}$ ) <sup>3</sup>	$V_{\text{Meso}}$ ( $\text{cm}^3 \text{g}^{-1}$ ) <sup>4</sup>	$F_{\text{Micro}}$ (%) <sup>5</sup>
NC	158	0.190	0.055	0.135	29
NC-KCl	903	0.686	0.348	0.338	51
NC-KOH	1030	0.659	0.401	0.258	61
NC-KCl-KOH	1034	0.634	0.398	0.236	63

<sup>1</sup>  $S_{\text{BET}}$  is the specific surface area determined by the BET method. <sup>2</sup>  $V_{\text{Total}}$  is the total pore volume. <sup>3</sup>  $V_{\text{Micro}}$  is the micropore volume. <sup>4</sup>  $V_{\text{Meso}}$  is the mesoporous volume. <sup>5</sup>  $F_{\text{Micro}}$  is the fraction of micropore volume to total pore volume.

Based on the above discussions, the CO<sub>2</sub> adsorption capacity of the sample was determined by the nitrogen content and the pore structure. By contrast, the latter played a more important role.

The micropore size distribution of typical samples was characterized by using the Harvath–Kawazoe (H–K) equation based on the N<sub>2</sub> adsorption and desorption data (Figure 11). Obviously, the micropores in the NC sample were very few, which is consistent with its small micropore volume presented in Table 2. The introduction of KCl in the R-F resin synthesis could promote the formation of more micropores and the micropore size ranged from 0.3–1.9 nm with a peak at 0.50 nm. Similar effect could be also observed when adding KOH in the carbonization process of the material. It's different from the NC-KCl sample that the NC-KOH sample had more micropores with smaller pore size and the peak value shifted left to 0.46 nm. The NC-KCl-KOH sample exhibited a nearly same micropore structure with the NC-KOH sample. It is noteworthy that the size of most micropores in the three samples activated by base and/or salt is smaller than 0.7 nm, and these pores were reported to support the CO<sub>2</sub> adsorption [48].

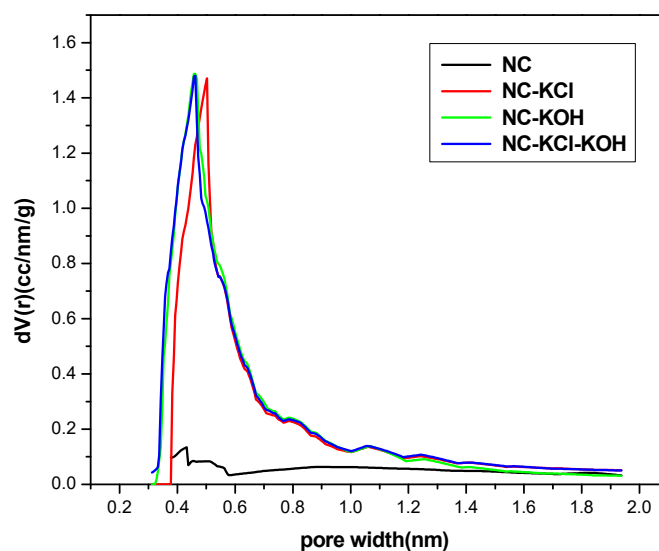


**Figure 11.** The micropore size distribution of typical samples.

The nitrogen bonding configurations were further studied by XPS and the N 1s spectra of typical samples are shown in Figure 12. Two signal peaks with binding energy at 398.5 and 400.3 eV were observed in all the samples except for NC-KCl-KOH sample. The peak at 398.5 eV could be assigned to pyridinic nitrogen and the peak at 400.3 eV to graphitic nitrogen [49]. It can be found that the ratio of pyridinic nitrogen to graphitic nitrogen was greatly influenced by the pre-treatment activation by

comparing the relative intensity of pyridinic and graphitic nitrogen peaks. The salt and base activation pre-treatment led to a decrease in the ratio of pyridinic nitrogen to graphitic nitrogen. In the case of NC-KCl-KOH sample, only the signal peak corresponding to graphitic nitrogen was observed, which suggested that graphitic nitrogen could behave as effective binding sites for CO<sub>2</sub>. It has been reported that different kinds of nitrogen functional groups have different degrees of effects on materials' CO<sub>2</sub> adsorption [32], which is also the reason for that the material's nitrogen content obtained by element analysis could not match its CO<sub>2</sub> adsorption performance very well.

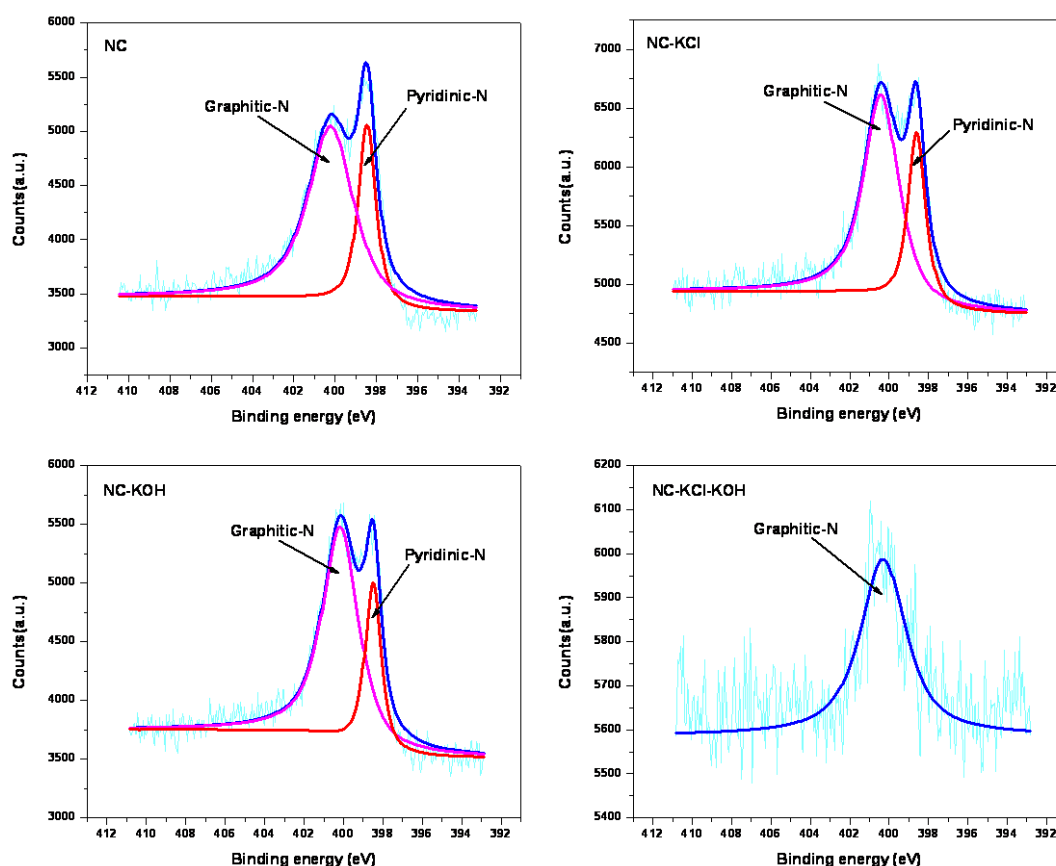


Figure 12. N1s XPS spectra of typical samples.

Finally, the surface morphology of typical samples and their precursors were analyzed by SEM and the results were shown in Figure 13. The morphology of the precursor without KCl activation took on like-lumps feature. When adding 0.75 g KCl in the precursor synthesis, the morphology could be changed to form uniform and close-connected small spheres. However, the surface of the NC and NC-KCl samples both consisted of carbon blocks with different size although the latter contained more carbon blocks with smaller size. Besides irregular carbon blocks, some uniformly small carbon spheres could be also observed when introducing 1.2 g KOH in the carbonization process of the precursor without KCl activation pretreatment, which could be attributed to the etch effect of base. Different from the above case, only uniformly small carbon spheres were obtained when the sample was co-activated by 0.75 KCl and 1.2 g KOH, which suggested a synergistic effect of base and salt activation pretreatment on the regulation of the morphology.

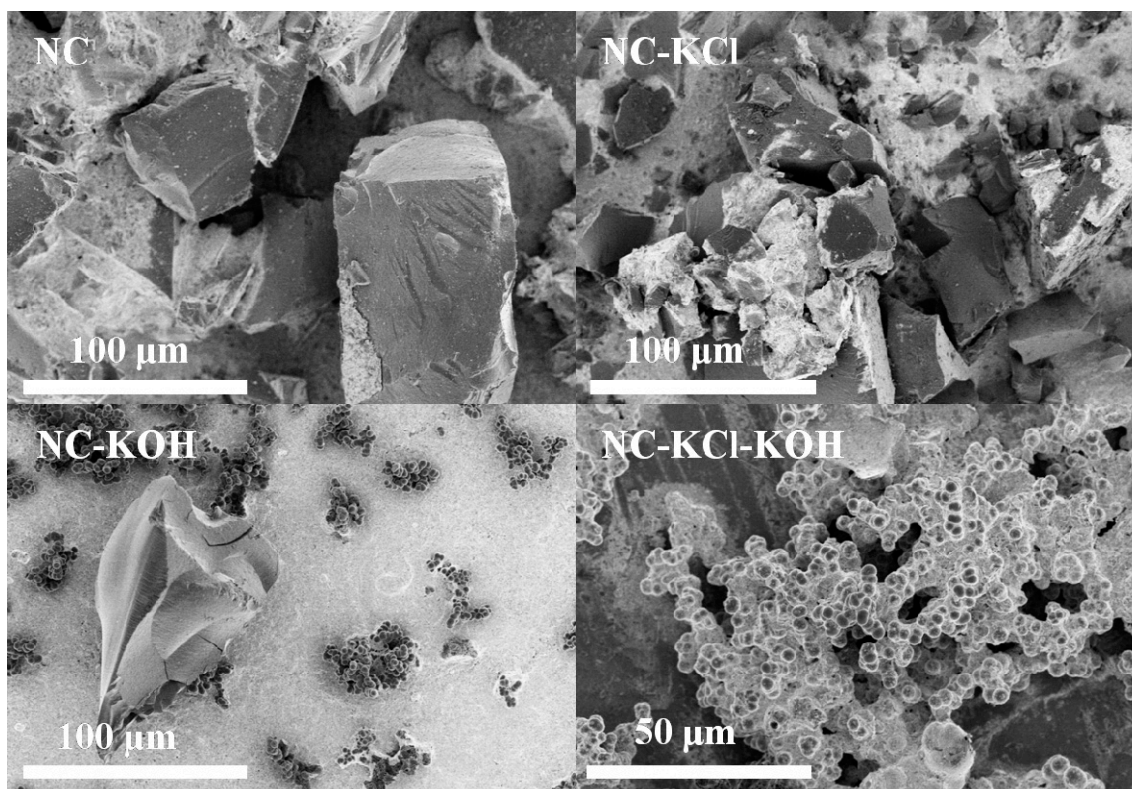


Figure 13. SEM image of typical samples and their precursors.

#### 4. Conclusions

In this work, a series of nitrogen-doped carbon materials with high CO<sub>2</sub> capture capacity were prepared by the ammoxidation of resorcinol-formaldehyde resin precursor with the aid of salt and/or base pretreatment activation. An obvious synergistic effect was observed between base and salt and the combination of 0.75 g KCl and 1.2 g KOH was proven to be the best combination. The sample co-activated by KCl and KOH exhibited the best CO<sub>2</sub> adsorption performance and 1 g typical NC-KCl-KOH sample could adsorb up to 167.15 mg CO<sub>2</sub>. The extensive characterization revealed that the introduction of KCl and KOH could increase the doped nitrogen content, change the nitrogen bonding configurations, enlarge the specific surface area and promote the formation of micropores with the size <0.7 nm. Therefore, the CO<sub>2</sub> adsorption capacity of the nitrogen doped carbon material should be co-influenced by the amount and type of doped nitrogen and the pore structure.

**Author Contributions:** Conceptualization, F.S.; Investigation, R.W.; Writing—original draft preparation, R.W., X.D. and F.S.; Writing—review and editing, R.W., X.D. and F.S.; Funding acquisition, F.S.

**Funding:** This research was funded by the National Natural Science Foundation of China, grant number (91745106, 21633013).

**Acknowledgments:** We thank the financial supports by the National Natural Science Foundation of China (91745106, 21633013).

**Conflicts of Interest:** The authors declare no conflict of interest.

#### References

1. Samanta, A.; Zhao, A.; Shimizu, G.K.H.; Sarkar, P.; Gupta, R. Post-combustion CO<sub>2</sub> capture using solid sorbents: A review. *Ind. Eng. Chem. Res.* **2011**, *51*, 1438–1463. [[CrossRef](#)]
2. Yang, H.; Xu, Z.; Fan, M.; Gupta, R.; Slimane, R.B.; Bland, A.E.; Wright, I. Progress in carbon dioxide separation and capture: A review. *J. Environ. Sci.* **2008**, *20*, 14–27. [[CrossRef](#)]

3. Jee, S.E.; Sholl, D.S. Carbon dioxide and methane transport in DDR zeolite insights from molecular simulations into carbon dioxide separations in small pore zeolites. *J. Am. Chem. Soc.* **2009**, *131*, 7896–7904. [[CrossRef](#)] [[PubMed](#)]
4. Su, F.; Lu, C.; Kuo, S.-C.; Zeng, W. Adsorption of CO<sub>2</sub> on amine-functionalized Y-type zeolites. *Energy Fuels* **2010**, *24*, 1441–1448. [[CrossRef](#)]
5. Zúkal, A.; Zones, S.I.; Kubů, M.; Davis, T.M.; Čejka, J. Adsorption of carbon dioxide on sodium and potassium forms of STI zeolite. *ChemPlusChem* **2012**, *77*, 675–681. [[CrossRef](#)]
6. Sánchez-Zambrano, K.; Lima Duarte, L.; Soares Maia, D.; Vilarrasa-García, E.; Bastos-Neto, M.; Rodríguez-Castellón, E.; Silva de Azevedo, D. CO<sub>2</sub> capture with mesoporous silicas modified with amines by double functionalization: assessment of adsorption/desorption cycles. *Materials* **2018**, *11*, 887. [[CrossRef](#)] [[PubMed](#)]
7. Zúkal, A.; Jagiello, J.; Mayerová, J.; Čejka, J. Thermodynamics of CO<sub>2</sub> adsorption on functionalized SBA-15 silica. NLDFT analysis of surface energetic heterogeneity. *Phys. Chem. Chem. Phys.* **2011**, *13*, 15468. [[CrossRef](#)]
8. Yu, J.; Le, Y.; Cheng, B. Fabrication and CO<sub>2</sub> adsorption performance of bimodal porous silica hollow spheres with amine-modified surfaces. *RSC Adv.* **2012**, *2*, 6784. [[CrossRef](#)]
9. Vilarrasa-García, E.; Cecilia, J.; Moya, E.; Cavalcante, C.; Azevedo, D.; Rodríguez-Castellón, E. “Low Cost” pore expanded SBA-15 functionalized with amine groups applied to CO<sub>2</sub> adsorption. *Materials* **2015**, *8*, 2495–2513. [[CrossRef](#)]
10. Li, Y.; Sun, N.; Li, L.; Zhao, N.; Xiao, F.; Wei, W.; Sun, Y.; Huang, W. Grafting of amines on ethanol-extracted SBA-15 for CO<sub>2</sub> adsorption. *Materials* **2013**, *6*, 981–999. [[CrossRef](#)] [[PubMed](#)]
11. Koirala, R.; Gunugunuri, K.R.; Pratsinis, S.E.; Smirniotis, P.G. Effect of zirconia doping on the structure and stability of CaO-based sorbents for CO<sub>2</sub> capture during extended operating cycles. *J. Phys. Chem. C* **2011**, *115*, 24804–24812. [[CrossRef](#)]
12. Wang, Q.; Tay, H.H.; Zhong, Z.; Luo, J.; Borgna, A. Synthesis of high-temperature CO<sub>2</sub> adsorbents from organo-layered double hydroxides with markedly improved CO<sub>2</sub> capture capacity. *Energy Environ. Sci.* **2012**, *5*, 7526. [[CrossRef](#)]
13. Broda, M.; Müller, C.R. Synthesis of highly efficient, Ca-Based, Al<sub>2</sub>O<sub>3</sub>-stabilized, carbon gel-templated CO<sub>2</sub> sorbents. *Adv. Mater.* **2012**, *24*, 3059–3064. [[CrossRef](#)] [[PubMed](#)]
14. Millward, A.R.; Yaghi, O.M. Metal-organic frameworks with exceptionally high capacity for storage of carbon dioxide at room temperature. *J. Am. Chem. Soc.* **2005**, *127*, 17998–17999. [[CrossRef](#)]
15. Junghans, U.; Kobalz, M.; Erhart, O.; Preißler, H.; Lincke, J.; Möllmer, J.; Krautscheid, H.; Gläser, R. A Series of robust copper-based triazolyl isophthalate MOFs: Impact of linker functionalization on gas sorption and catalytic activity. *Materials* **2017**, *10*, 338. [[CrossRef](#)]
16. Torrisi, A.; Bell, R.G.; Mellot-Draznieks, C. Functionalized MOFs for enhanced CO<sub>2</sub> capture. *Cryst. Growth Des.* **2010**, *10*, 2839–2841. [[CrossRef](#)]
17. Cao, Y.; Zhang, H.; Song, F.; Huang, T.; Ji, J.; Zhong, Q.; Chu, W.; Xu, Q. UiO-66-NH<sub>2</sub>/GO composite: synthesis, characterization and CO<sub>2</sub> adsorption performance. *Materials* **2018**, *11*, 589. [[CrossRef](#)]
18. Altintas, C.; Avci, G.; Daglar, H.; NematVesali Azar, A.; Velioglu, S.; Erucar, I.; Keskin, S. Database for CO<sub>2</sub> separation performances of MOFs based on computational materials screening. *ACS Appl. Mater. Interfaces* **2018**, *10*, 17257–17268. [[CrossRef](#)] [[PubMed](#)]
19. Allen, A.; Wong-Ng, W.; Cockayne, E.; Culp, J.; Matranga, C. Structural basis of CO<sub>2</sub> adsorption in a flexible metal-organic framework material. *Nanomaterials* **2019**, *9*, 354. [[CrossRef](#)] [[PubMed](#)]
20. Wahby, A.; Ramos-Fernández, J.M.; Martínez-Escandell, M.; Sepúlveda-Escribano, A.; Silvestre-Albero, J.; Rodríguez-Reinoso, F. High-surface-area carbon molecular sieves for selective CO<sub>2</sub> adsorption. *ChemSusChem* **2010**, *3*, 974–981. [[CrossRef](#)]
21. Silvestre-Albero, J.; Wahby, A.; Sepúlveda-Escribano, A.; Martínez-Escandell, M.; Kaneko, K.; Rodríguez-Reinoso, F. Ultrahigh CO<sub>2</sub> adsorption capacity on carbon molecular sieves at room temperature. *Chem. Commun.* **2011**, *47*, 6840. [[CrossRef](#)]
22. Maroto-Valer, M.M.; Tang, Z.; Zhang, Y. CO<sub>2</sub> capture by activated and impregnated anthracites. *Fuel Process. Technol.* **2005**, *86*, 1487–1502. [[CrossRef](#)]

23. Alghamdi, A.; Alshahrani, A.; Khadary, N.; Alharthi, F.; Alattas, H.; Adil, S. Enhanced CO<sub>2</sub> adsorption by nitrogen-doped graphene oxide sheets (N-GOs) prepared by employing polymeric precursors. *Materials* **2018**, *11*, 578. [[CrossRef](#)]
24. Chiang, Y.-C.; Hsu, W.-L.; Lin, S.-Y.; Juang, R.-S. Enhanced CO<sub>2</sub> adsorption on activated carbon fibers grafted with nitrogen-doped carbon nanotubes. *Materials* **2017**, *10*, 511. [[CrossRef](#)] [[PubMed](#)]
25. Bhagiyalakshmi, M.; Hemalatha, P.; Ganesh, M.; Mei, P.M.; Jang, H.T. A direct synthesis of mesoporous carbon supported MgO sorbent for CO<sub>2</sub> capture. *Fuel* **2011**, *90*, 1662–1667. [[CrossRef](#)]
26. Balahmar, N.; Mitchell, A.C.; Mokaya, R. Generalized mechanochemical synthesis of biomass-derived sustainable carbons for high performance CO<sub>2</sub> storage. *Adv. Energy Mater.* **2015**, *5*, 1500867. [[CrossRef](#)]
27. Bermúdez, J.; Dominguez, P.; Arenillas, A.; Cot, J.; Weber, J.; Luque, R. CO<sub>2</sub> separation and capture properties of porous carbonaceous materials from leather residues. *Materials* **2013**, *6*, 4641–4653. [[CrossRef](#)]
28. Sevilla, M.; Al-Jumaily, A.S.M.; Fuertes, A.B.; Mokaya, R. Optimization of the pore structure of biomass-based carbons in relation to their use for CO<sub>2</sub> capture under low- and high-pressure regimes. *ACS Appl. Mater. Interfaces* **2018**, *10*, 1623–1633. [[CrossRef](#)]
29. Yue, L.; Xia, Q.; Wang, L.; Wang, L.; DaCosta, H.; Yang, J.; Hu, X. CO<sub>2</sub> adsorption at nitrogen-doped carbons prepared by K<sub>2</sub>CO<sub>3</sub> activation of urea-modified coconut shell. *J. Colloid Interface Sci.* **2018**, *511*, 259–267. [[CrossRef](#)]
30. Kou, J.; Sun, L.-B. Fabrication of nitrogen-doped porous carbons for highly efficient CO<sub>2</sub> capture: rational choice of a polymer precursor. *J. Mater. Chem. A* **2016**, *4*, 17299–17307. [[CrossRef](#)]
31. Shao, L.; Liu, M.; Huang, J.; Liu, Y.-N. CO<sub>2</sub> capture by nitrogen-doped porous carbons derived from nitrogen-containing hyper-cross-linked polymers. *J. Colloid Interface Sci.* **2018**, *513*, 304–313. [[CrossRef](#)]
32. Hao, G.-P.; Li, W.-C.; Qian, D.; Lu, A.-H. Rapid synthesis of nitrogen-doped porous carbon monolith for CO<sub>2</sub> capture. *Adv. Mater.* **2010**, *22*, 853–857. [[CrossRef](#)] [[PubMed](#)]
33. Plaza, M.G.; Pevida, C.; Arenillas, A.; Rubiera, F.; Pis, J.J. CO<sub>2</sub> capture by adsorption with nitrogen enriched carbons. *Fuel* **2007**, *86*, 2204–2212. [[CrossRef](#)]
34. Li, X.; Wang, H.; Robinson, J.T.; Sanchez, H.; Diankov, G.; Dai, H. Simultaneous nitrogen doping and reduction of graphene oxide. *J. Am. Chem. Soc.* **2009**, *131*, 15939–15944. [[CrossRef](#)]
35. Pevida, C.; Plaza, M.G.; Arias, B.; Feroso, J.; Rubiera, F.; Pis, J.J. Surface modification of activated carbons for CO<sub>2</sub> capture. *Appl. Surf. Sci.* **2008**, *254*, 7165–7172. [[CrossRef](#)]
36. Plaza, M.G.; Rubiera, F.; Pis, J.J.; Pevida, C. Amoxidation of carbon materials for CO<sub>2</sub> capture. *Appl. Surf. Sci.* **2010**, *256*, 6843–6849. [[CrossRef](#)]
37. Mangun, C.L.; Benak, K.R.; Economy, J.; Foster, K.L. Surface chemistry, pore sizes and adsorption properties of activated carbon fibers and precursors treated with ammonia. *Carbon* **2001**, *39*, 1809–1820. [[CrossRef](#)]
38. Li, G.; Wang, Z. Microporous polyimides with uniform pores for adsorption and separation of CO<sub>2</sub> gas and organic vapors. *Macromolecules* **2013**, *46*, 3058–3066. [[CrossRef](#)]
39. Park, J.; Nabae, Y.; Hayakawa, T.; Kakimoto, M.-a. Highly selective two-electron oxygen reduction catalyzed by mesoporous nitrogen-doped carbon. *ACS Catal.* **2014**, *4*, 3749–3754. [[CrossRef](#)]
40. Tian, Z.; Huang, J.; Zhang, X.; Shao, G.; He, Q.; Cao, S.; Yuan, S. Ultra-microporous N-doped carbon from polycondensed framework precursor for CO<sub>2</sub> adsorption. *Microporous Mesoporous Mater.* **2018**, *257*, 19–26. [[CrossRef](#)]
41. Yin, F.; Zhuang, L.; Luo, X.; Chen, S. Simple synthesis of nitrogen-rich polymer network and its further amination with PEI for CO<sub>2</sub> adsorption. *Appl. Surf. Sci.* **2018**, *434*, 514–521. [[CrossRef](#)]
42. De Souza, L.K.C.; Wickramaratne, N.P.; Ello, A.S.; Costa, M.J.F.; da Costa, C.E.F.; Jaroniec, M. Enhancement of CO<sub>2</sub> adsorption on phenolic resin-based mesoporous carbons by KOH activation. *Carbon* **2013**, *65*, 334–340. [[CrossRef](#)]
43. Yu, J.; Guo, M.; Muhammad, F.; Wang, A.; Yu, G.; Ma, H.; Zhu, G. Simple fabrication of an ordered nitrogen-doped mesoporous carbon with resorcinol-melamine-formaldehyde resin. *Microporous Mesoporous Mater.* **2014**, *190*, 117–127. [[CrossRef](#)]
44. Lee, S.-Y.; Park, S.-J. Determination of the optimal pore size for improved CO<sub>2</sub> adsorption in activated carbon fibers. *J. Colloid Interface Sci.* **2013**, *389*, 230–235. [[CrossRef](#)] [[PubMed](#)]
45. Wickramaratne, N.P.; Jaroniec, M. Importance of small micropores in CO<sub>2</sub> capture by phenolic resin-based activated carbon spheres. *J. Mater. Chem. A* **2013**, *1*, 112–116. [[CrossRef](#)]

46. Meng, L.-Y.; Park, S.-J. Effect of heat treatment on CO<sub>2</sub> adsorption of KOH-activated graphite nanofibers. *J. Colloid Interface Sci.* **2010**, *352*, 498–503. [[CrossRef](#)] [[PubMed](#)]
47. Li, Y.; Ben, T.; Zhang, B.; Fu, Y.; Qiu, S. Ultrahigh gas storage both at low and high pressures in KOH-activated carbonized porous aromatic frameworks. *Sci. Rep.* **2013**, *3*, 2420. [[CrossRef](#)]
48. Sánchez-Sánchez, Á.; Suárez-García, F.; Martínez-Alonso, A.; Tascón, J.M.D. Influence of porous texture and surface chemistry on the CO<sub>2</sub> adsorption capacity of porous carbons: acidic and basic site interactions. *ACS Appl. Mater. Interfaces* **2014**, *6*, 21237–21247. [[CrossRef](#)]
49. Rehman, A.; Park, S.-J. Comparative study of activation methods to design nitrogen-doped ultra-microporous carbons as efficient contenders for CO<sub>2</sub> capture. *Chem. Eng. J.* **2018**, *352*, 539–548. [[CrossRef](#)]
50. Sethia, G.; Sayari, A. Comprehensive study of ultra-microporous nitrogen-doped activated carbon for CO<sub>2</sub> capture. *Carbon* **2015**, *93*, 68–80. [[CrossRef](#)]
51. Yang, H.; Cui, X.; Deng, Y.; Shi, F. Highly efficient carbon catalyzed aerobic selective oxidation of benzylic and allylic alcohols under transition-metal and heteroatom free conditions. *RSC Adv.* **2014**, *4*, 59754–59758. [[CrossRef](#)]
52. Yang, H.; Cui, X.; Dai, X.; Deng, Y.; Shi, F. Carbon-catalysed reductive hydrogen atom transfer reactions. *Nat. Commun.* **2015**, *6*, 6478. [[CrossRef](#)] [[PubMed](#)]
53. Liu, J.; Qiao, S.Z.; Liu, H.; Chen, J.; Orpe, A.; Zhao, D.; Lu, G.Q.M. Extension of the stöber method to the preparation of monodisperse resorcinol-formaldehyde resin polymer and carbon spheres. *Angew. Chem. Int. Ed.* **2011**, *50*, 5947–5951. [[CrossRef](#)] [[PubMed](#)]
54. Azambre, B.; Zenboury, L.; Koch, A.; Weber, J.V. Adsorption and desorption of NO<sub>x</sub> on commercial ceria-zirconia (Ce<sub>x</sub>Zr<sub>1-x</sub>O<sub>2</sub>) mixed oxides: a combined TGA, TPD-MS, and DRIFTS study. *J. Phys. Chem. C* **2009**, *113*, 13287–13299. [[CrossRef](#)]
55. Ebner, A.D.; Reynolds, S.P.; Ritter, J.A. Nonequilibrium kinetic model that describes the reversible adsorption and desorption behavior of CO<sub>2</sub> in a K-promoted hydrotalcite-like compound. *Ind. Eng. Chem. Res.* **2007**, *46*, 1737–1744. [[CrossRef](#)]
56. Xu, X.; Song, C.; Andresen, J.M.; Miller, B.G.; Scaroni, A.W. Novel polyethylenimine-modified mesoporous molecular sieve of MCM-41 type as high-capacity adsorbent for CO<sub>2</sub> capture. *Energy Fuels* **2002**, *16*, 1463–1469. [[CrossRef](#)]

